Highly permeable and mechanically robust silicon carbide hollow fiber membranes

Patrick de Wit[a], Emiel J. Kappert[a], Theresa Lohaus[b], Matthias Wessling[b,c], Arian Nijmeijer[a], Nieck E. Benes[a,*]

[a]*Inorganic Membranes, Department of Science and Technology, MESA+ Institute for Nanotechnology, University of Twente, P.O. Box 217, 7500 AE Enschede, The Netherlands*
[b]*RWTH Aachen University, AVT.CVT - Chair of Chemical Product and Process Engineering, Turmstr. 46, 52064 Aachen, Germany*
[c]*DWI - Leibniz Institute for Interactive Materials, Forckenbeckstr. 50, 52074 Aachen, Germany*

Abstract

Silicon carbide (SiC) membranes have shown large potential for applications in water treatment. Being able to make these membranes in a hollow fiber geometry allows for higher surface-to-volume ratios. In this study, we present a thermal treatment procedure that is tuned to produce porous silicon carbide hollow fiber membranes with sufficient mechanical strength. Thermal treatments up to 1500 °C in either nitrogen or argon resulted in relatively strong fibers, that were still contaminated with residual carbon from the polymer binder. After treatment at a higher temperature of 1790 °C, the mechanical strength had decreased as a result of carbon removal, but after treatments at even higher temperature of 2075 °C the SiC-particles sinter together, resulting in fibers with mechanical strengths of 30 MPa to 40 MPa and exceptionally high water permeabilities of 50 000 L m^{-2} h^{-1} bar^{-1}. Combined with the unique chemical and thermal resistance of silicon carbide, these properties make the fibers suitable microfiltration membranes or as a membrane support for application under demanding conditions.

Keywords: silicon carbide, inorganic porous hollow fiber, water treatment, oil-water separation

1. Introduction

The outstanding mechanical integrity and chemical stability of silicon carbide has resulted in its use in various applications in which the material has to resist harsh conditions, such as diesel particulate filters [1], catalyst carriers [2], and sensors that are used at extreme pHs [3]. Whereas silicon carbide membranes also have been proposed for gas separation [4–8], the application of silicon carbide membranes for liquid applications has received little attention in literature. In 2011, Hofs et al demonstrated the superb fouling resistance of silicon carbide membranes in the treatment of surface water [9]. Several companies claimed that this low-fouling behaviour extents to the harsh conditions of oil/water separations [10–12].

Until now, silicon carbide membranes have been limited to flat [13], tubular [4, 14] and multichannel [5] geometries. All these geometries have a comparatively low surface-to-volume ratio in comparison with hollow fibers. The synthesis of inorganic hollow fibers has seen increasing attention during the last decade [15–18], but the few silicon carbide fibers that have been produced showed an undesirable pore structure [19, 20] or poor mechanical stability [21].

In the present paper, we developed a procedure for the fabrication of mechanically robust, porous silicon carbide hollow fibers via dry-wet spinning. The paper elaborates on the effects of the thermal treatment on the structure and properties of the obtained fibers, demonstrating that a felicitous thermal treatment is of key importance for the successful synthesis of highly permeable and mechanically robust silicon carbide hollow fibers.

2. Experimental

2.1. Materials

α-Silicon carbide powders with a mean size of 0.4 and 0.6 µm were supplied by Liqtech International AS (Denmark). Polyethersulfone (PES, Ultrason® E 6020 P, BASF), N-methyl-2-pyrrolidone (NMP, <99.5%, Sigma Aldrich) and de-ionized water (<18.2 MΩ cm^{-1},

*Corresponding author
Email address: N.E.Benes@utwente.nl (Nieck E. Benes)

Table 1: Spinning conditions

Condition	Value
Bore Liquid	H_2O
Coagulation bath	H_2O
Extrusion pressure	2 bar
Air gap	3 cm
Bore liquid flow rate	7 mL min^{-1}
Diameter spinneret	OD/ID=2.0 mm/0.8 mm

Milli-Q Advantage A10, Millipore) were used for dry-wet spinning. Prior to use, PES was dried overnight at 80 °C; all other chemicals were used as received. Sintering was carried out in argon (4.5) or nitrogen (2.8) gas atmosphere (Praxair).

2.2. Dry-wet spinning

The spinning dope composition was based on prior work [22]. Silicon carbide powders were mixed in a 1:5 weight ratio (0.4:0.6 µm), added to NMP and treated ultrasonically for 30 min. PES was added in multiple steps to this mixture, allowing the PES to dissolve before the next amount was added. The resulting spinning mixture was composed of 36 wt% of SiC, 50 wt% of NMP and 14 wt% of PES. After stirring overnight, vacuum was applied for 30 min and the mixture was left overnight to degas.

For the dry-wet spinning, the mixture was forced through a spinneret by pressuring a stainless-steel vessel with nitrogen. The spinning conditions are given in Table 1; full details on the spinning setup can be found elsewhere [21]. After spinning, the fibers were stretched (1 cm m^{-1}) and dried prior to sintering.

2.3. Thermal treatment

Thermal treatments up to 1500 °C were carried out in a STF 16/610 tubular furnace (Carbolite) equipped with an alumina working tube. Samples were loaded in SiC crucibles and thermally treated according to the programs given in Table 2. Prior to sintering, the system was evacuated and refilled with either argon or nitrogen three times, followed by sintering under a sweep flow of 100 mL min^{-1}.

High-temperature sintering (1500 °C to 2075 °C) was carried out at Liqtech Industries A/S, Denmark, where the fibers were co-sintered with a running production batch. All high-temperature sintering was carried out under argon; prior to shipping for high-temperature sintering, the samples were pre-sintered at 1500 °C for 2 h in argon.

Table 2: Overview of the used sintering programs. For all experiments, a 5 °C min^{-1} heating rate was employed.

Name	Sintering	Atmosphere
300-N_2	1 h at 300 °C	Nitrogen
1000-N_2	1 h at 300 °C, 3 h at 1000 °C	
1500-N_2	1 h at 300 °C, 3 h at 1500 °C	
300-Ar	1 h at 300 °C	Argon
1000-Ar	1 h at 300 °C, 3 h at 1000 °C	
1500-Ar	1 h at 300 °C, 3 h at 1500 °C	
1790-Ar*	6 h at 1790 °C	
2075-Ar*	0.75 h at 2075 °C	

** Sample sintered at Liqtech, Denmark. Samples were pre-sintered according to program 1500-Ar.*

Fiber mass (m), length (l) and diameter (d) were determined per fiber prior to and after thermal treatment to allow for paired comparison.

2.4. Characterization

2.4.1. SEM-EDS

The cross section morphology, the wall thickness and semi-quantitative elemental analysis of green and sintered fibers were obtained with a JSM-6010LA scanning electron microscope equipped with an energy dispersive spectrometer (Jeol). To obtain a clean fracture, the green compacts were soaked in liquid nitrogen before fracturing. The samples were gold-sputtered (13 mA, 3 min) before SEM photos were taken. The EDS spectra were obtained from a cross-section of the non-sputtered fibers in low-vacuum mode.

2.4.2. TGA-MS

Thermogravimetric analysis (TGA) was performed on a STA 449 F3 Jupiter® (Netzch) fitted with a TG-only sample holder. Measurements were performed under 70 mL min^{-1} argon at a heating rate of 20 °C min^{-1} from room temperature to 1500 °C. Temperature correction by melting standard and a blank correction with an empty cup were carried out prior to the measurements. Small fragments of dried fibers were used as sample and their mass was determined externally.

Gases evolving during the thermogravimetric analysis were transferred to a mass spectrometer (MS, QMS 403 D Aëolos®, Netzsch) by a glass capillary. TGA and MS start times were synchronized; no correction was applied for the time offset caused by the transfer line time (estimated <30 s, systematic offset). First, a bar graph scan for m/z = 1—100 amu was performed to

determine the evolving m/z-numbers (data not included here). The detected m/z-numbers (2, 12, 14—18, 20, 26-30, 32, 36, 38, 40, 44, 48—52, 56, 60—61, 64, 67—68) were selected and recorded more accurately in multiple-ion-detection mode, with a dwell of 0.5 s per m/z-value and a resolution of 50.

2.4.3. Clean water permeation

The clean water flux was measured using an OSMO Inspector 2 (Convergence, Netherlands). Experiments were carried out in dead-end mode under constant flux operation with three different flux settings for each fiber. Custom-made single-fiber modules were used made out of Plexiglass tubing and sealed with PUR435/PUR-N 2-component glue (Intercol, Germany).

The permeate flow Φ_v ($\mathrm{L\,h^{-1}}$) was recorded as a function of the transmembrane pressure. The pressure drop over the fiber is assumed to be negligible. The permeability was calculated using eq. 1, where A is the effective membrane area.

$$\Pi = \frac{\Phi_v}{(p_{\mathrm{feed}} - p_{\mathrm{permeate}}) \cdot A} \tag{1}$$

2.4.4. Conductivity

Electrical conductivity was measured using a home-build 4-probe conductivity meter. Current was applied at the outer probes that were 7 cm apart; the voltage drop was measured with two inner probes 3 cm apart. Measurements were performed at room temperature on three different spots at each fiber.

2.4.5. Mercury intrusion porosimetry

The volume of mercury intruded was measured as function of the pressure using a Poremaster PM-33-14 (Quantachrome®). The helium density was measured using an AccuPyc II 1340 gas displacement analyzer (Micromeritics). Pressure p and volume mercury intruded V_{Hg} were recorded and data processing was performed using Matlab® [23]. The pore diameter corresponding to a certain pressure is calculated using Washburn's equation [24] (Supplementary Information). The volume based pore size distribution is calculated via eq. 2.

$$D_v(r) = \frac{dV_{\mathrm{Hg}}}{dp}\left|\frac{p^2}{2\gamma\cos\theta}\right| \tag{2}$$

The porosity is computed by combining apparent density measured using helium ρ_{He} and mercury ρ_{Hg} and calculated using equation 3.

$$\varepsilon = 100\left[1 - \frac{\rho_{\mathrm{Hg}}}{\rho_{\mathrm{He}}}\right] \tag{3}$$

2.4.6. Mechanical strength

Mechanical testing (4-point bending test) was carried out according to ASTM C1161-02 [25] using a 5564A mechanical testing bench (Instron). Sintered fibers were cut to a length of 5 cm, and tested with a crosshead speed of $2\,\mathrm{mm\,min^{-1}}$ at room temperature. The force and deflection curves were measured and subsequently the bending strength for sample j was calculated using

$$\sigma_j = \frac{16F_jKd_{o,j}}{\pi\left(d_{o,j}^4 - d_{i,j}^4\right)} \tag{4}$$

where F_j is the force at fracture, K half the difference between outer and inner span (5 mm) and $d_{i,j}$ and $d_{o,j}$ are the inner and outer diameter of the hollow fiber j at its fracture site. The error in the calculated bending strength was estimated using $\Delta F = \pm 0.5\%$, $\Delta d_i = \Delta d_o = 20\,\mu\mathrm{m}$ and $\Delta K = 50\,\mu\mathrm{m}$. For each fiber a minimum of 20 measurements were taken and the obtained bending strengths were fitted by a Weibull cumulative probability function, where the characteristic strength σ_θ and the shape parameter m_{shape} are used as fitting parameters (full details in the supplementary information).

3. Results and discussion

Figure 1 provides a set of pictures that show the fiber morphology before and after thermal treatments at various temperatures. Figure 1B and 1C display the fiber morphology of green hollow fibers after drying. The via dry-wet spinning prepared fiber consists of a PES network that is loaded with silicon carbide particles and has an asymmetric structure with finger-like voids at the lumen side and a sponge-like outer layer. Such a morphology is typical for inorganic fibers [15, 26]. Figure 1C shows the presence of 10 µmsized particles dispersed throughout the fiber. A close-up of these particles (not shown here) indicated that the grains are presumably aggregates/agglomerates of smaller silicon carbide grains.

Figure 1D-F show that sintering at temperatures of 1500 °C to 2075 °C has no apparent effect on the morphology of the silicon carbide fibers. The finger-like voids and sponge-like structure are both preserved. However, at temperatures in excess of 1790 °C, the sponge-like layer develops into a more open structure, in which the individual grains are clearly visible (see Figure 4 for close-up SEM images). The minor changes in morphology also reflected in the small changes in the radial dimensions between the green and the sintered fibers. Prior to sintering, the dried fibers had an outer diameter of 1.78 mm ± 0.02 mm. The level of shrinkage in radial ($d_{\mathrm{sintered}}/d_{\mathrm{green}}$) and longitudinal ($l_{\mathrm{sintered}}/l_{\mathrm{green}}$)

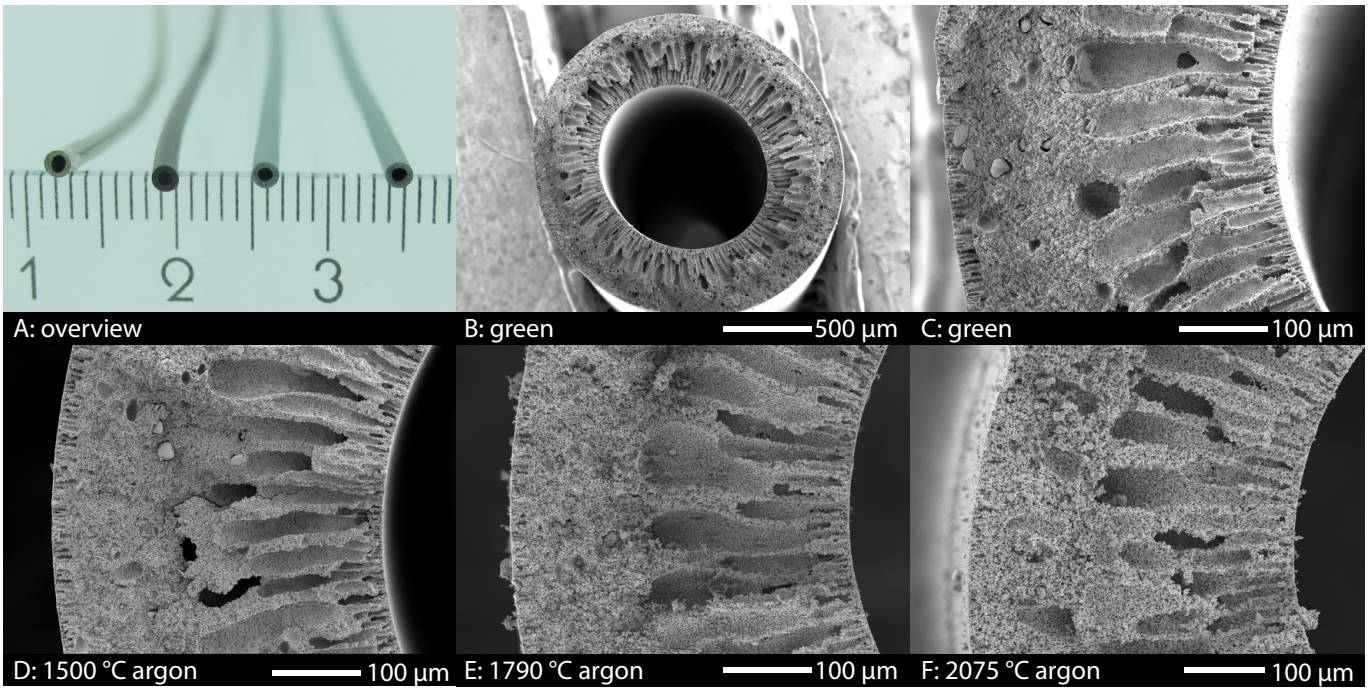

Figure 1: Photo of, from left to right, a green, sintered at 1500 °C, sintered at 1790 °C, sintered fiber 2075 °C (A), and cross-sectional images of a green (B), a green (C), 1500-Ar (D), 1790-Ar (E) and 2075-Ar (F) sintered fibers.

directions as a result of sintering at 2075 °C was limited to less than 5% and 8%, respectively (See the Supplementary Information). No difference was observed between sintering in argon or nitrogen atmospheres.

3.1. Thermal treatment

The mass loss of the green hollow fibers upon heating and the gases that have concurrently evolved are shown in Figure 2 for heating under argon up to 1500 °C (left panel), and for a consecutive 8 h dwell at 1500 °C (right panel). At lower temperatures (25 °C to 250 °C), minor mass loss is recorded that is accompanied by the release of water. This mass loss is attributed to the further drying of the SiC fibers. A second mass loss step is recorded at intermediate temperatures (450 °C to 650 °C), where SO_2, CO, CO_2 and water are the main gases emitted, followed by a minor mass loss concurring with release of methane, CO and CO_2 at 750 °C. This observed decomposition process matches closely to the reported decomposition of PES under an argon atmosphere [27–29], indicating that the presence of the silicon carbide has had no (apparent) effect on the decomposition of the PES.

Further mass loss is recorded at temperatures exceeding 1150 °C. This mass loss continues up to 1500 °C and persists for a full 8 h dwell period at this temperature. Mainly CO and CO_2 evolve during this step. As the reaction atmosphere is free of oxygen, the formation of CO and CO_2 is attributed to the following reaction [30, 31]:

$$SiO_2(g) + 3\,C(s) \longrightarrow SiC(s) + 2\,CO(g) \qquad (5)$$

The silica originates from impurities in the silicon carbide [32]. The production of CO_2 would be the result of only two carbon atoms reacting with the silica. The reaction between silica and silicon carbide is reported to be inhibited at these temperatures in the presence of free carbon [33]. The rate of reaction (5) is controlled by the diffusion of CO through the SiC fiber wall [31]. Among the main parameters that influence the rate of this process are the porosity, tortuosity and sample thickness of the material. In this respect, the fiber morphology — having a bore and large voids — would result in shorter times required for the thermal treatment than those required for a dense or mesoporous silicon carbide sample.

In Figure 3A, the mass of the fibers is shown after thermal treatment in nitrogen or argon. Because of the temperature limitations of the TG-apparatus and tubular furnaces, the temperature treatments at higher temperatures (>1500 °C) were performed in an industrial

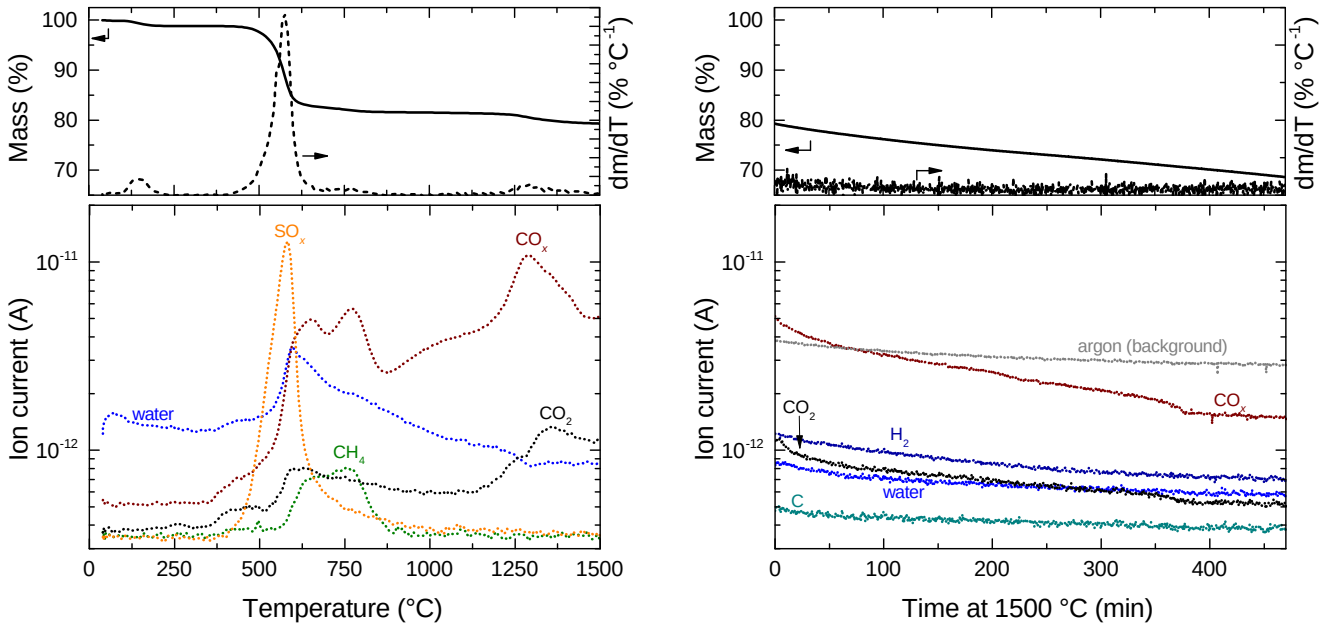

Figure 2: TGA-MS data of the thermal processing of SiC hollow fibres under argon with (A) a heating rate of 20 °C/ min followed by (B) a 8 h dwell at 1500 °C.

furnace, in which the fibers are co-fired along with the standard production batch. The results obtained up to 1500 °C are in excellent agreement with the previously discussed TG-experiments.

However, at temperatures above 1500 °C, a deviation from the mass loss trend is observed. At these temperatures, the fiber mass increases slowly with increasing sintering temperature. Mass conservation dictates that this increase in mass results from reactions with the atmosphere in the furnace. This cannot be the inert argon gas. It is known that the vapour pressure of silica is non-negligible at these temperatures, and that silica originating from the co-fired samples and/or the furnace can be deposited onto the samples. At the fiber, this silica can then react with the free carbon through reaction (5), yielding silicon carbide and carbon monoxide. At these high temperatures, an opposite reaction, in which silicon carbide reacts with the silica can occur as well [32]. The resulting silicon oxide will either be removed in the vapour phase, or disproportionate into silica and silicon at room temperature [34].

To test this hypothesis, the electrical conductivity of the silicon carbon fibers was measured after sintering. The electrical conductivity of amorphous carbon (up to 10^6 S m^{-1}) is multiple orders of magnitude higher than that of silicon carbide (down to 10^{-4} S m^{-1} under a nitrogen atmosphere) or voids [35, 36]. Hence, the deposition of silicon dioxide and the removal of carbon via reaction 5 should result in a sharp decline in the conductivity of the fibers. In Figure 3B, the electrical conductivity is given for fibers that have been treated under nitrogen or argon at various temperatures. The high electrical conductivity of the samples up to 1500 °C demonstrates that carbon is present and forms a percolative pathway through the material. Fitting of the data with a Bruggeman Effective Medium Approximation proved to be impossible, which demonstrates that the carbon is not present in the form of spherical inclusions, but more likely forms a film that surrounds the silicon carbide particles.

Above 1500 °C, the large drop in conductivity indicates the removal of the carbon from the fibers. To verify the presence of carbon in the 1500-Ar fiber, and the absence of carbon in the 2075-Ar fiber, these fibers were measured with TGA under air. The TGA-runs give a clear indication for the presence of 13.5 wt% residual carbon in the 1500-Ar fiber, and the absence of residual carbon in the 2075-Ar fiber (see the Supplementary Information).

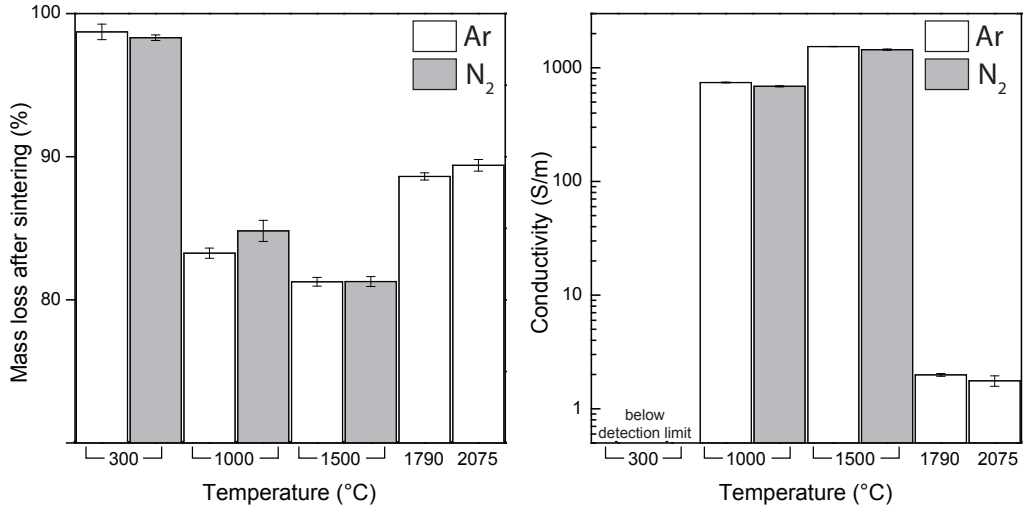

Figure 3: : (A) Final mass after thermal treatment (with 95% confidence interval) after sintering at certain temperatures and (B) conductivity after sintering at certain temperature. A full explanation of the thermal treatment steps is given in the text.

3.2. Microstructure of the treated SiC fibers

3.2.1. Scanning Electron Micrographs

Figure 4 shows the microstructure of the hollow fibers as a function of sintering temperature 1500 °C to 2400 °C). The microstructures of the fibers sintered at 1500 °C (Figure 4A and B) reveal submicron silicon carbide particles, still bound together by the residual carbon. No significant sintering has taken place, which is as expected for the comparatively short holding time of 2 h just above the sintering temperature (T_{Tamman} ~ 1250 °C). At higher temperatures, sintering is evident from the significant grain growth that is a consequence of Ostwald ripening (1790 °C in Figure 4C and 2075 °C in Figure 4D). The grains grow from loose grains, smaller than 0.5 µm in size, to strongly necked particles of approximately 2 µm at 2075 °C, forming an interconnected pore structure with large-sized pores. This degree of grain growth agrees well with reported morphologies of synthesized SiC substrates at comparable temperatures and without the use sintering additives. [1, 4].

3.2.2. Pore size distribution

Figure 5 shows the volume-based pore size distribution of fibers sintered under argon. It can be seen that the median pore size increases with increasing sintering temperature. The green fiber shows an apparent median pore size of 125 nm, consisting of both pores in the polymeric matrix and voids between the ceramic particles. After sintering at 1500 °C many of the smaller pores disappear as the polymer is converted into elemental carbon — leaving only the voids between the ceramic particles. This results in a bell-shaped pore size distribution with a median pore size of 500 nm. Still, a considerable amount of residual carbon is present in this fiber, as a subsequent oxidation step further opens up the pores in the 100 nm to 500 nm range (see the Supplementary Information).

Table 3: Porosity for green and sintered fibers, including standard error (see the Supplementary Information for details about the error analysis)

Sample	Porosity
Green	62.8±9.7
SiC1500Ar	64.4±6.5
SiC1790Ar	70.0±4.7
SiC2075Ar	63.5±4.8

At higher temperatures (1790 °C to 2075 °C), strong broadening of the pore size is observed, combined with a shift of the poresize to larger pores (>1000 nm). The increase in pore size agrees well with the observed increase in particle size (Figure 4). The change in pore size does not result in a strong change in the fiber' porosity (Table 3), as the porosity indicates there is no significant densification, even at higher sintering temperatures.

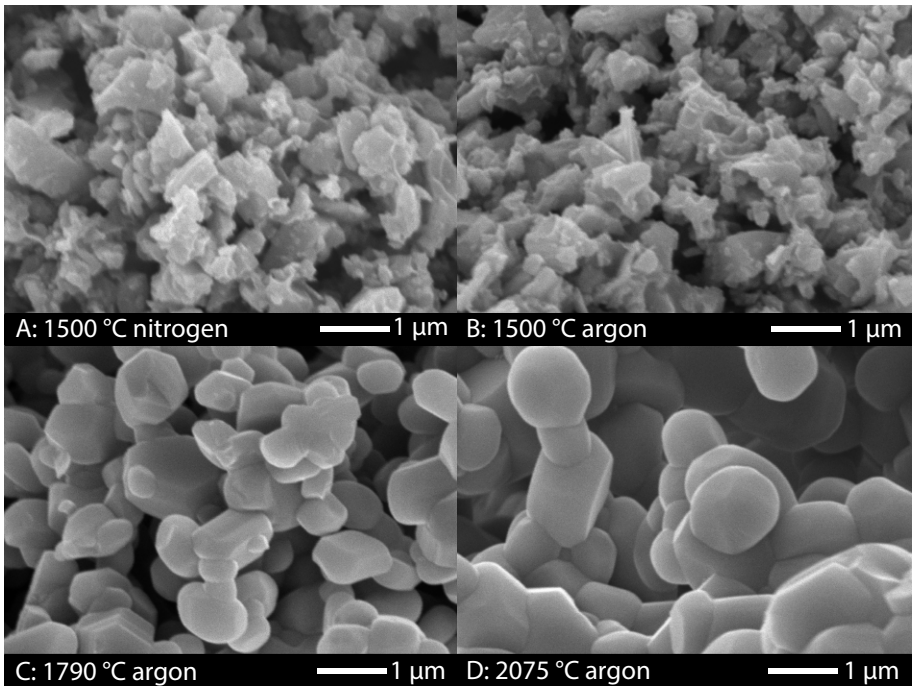

Figure 4: Cross section microstructure for sintered silicon carbide fibers. Details about the heat treatment can be found in Table 2. 1500 °C sintered fibers in nitrogen (A) and argon (B). 1790 °C (C), 2075 °C (D) were sintered in argon atmosphere.

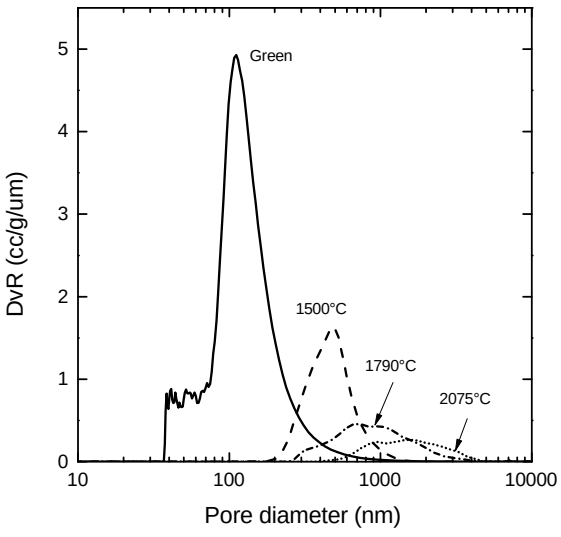

Figure 5: Volume—based pore size distribution by mercury intrusion for various sintering temperatures under argon atmosphere.

3.3. Properties

3.3.1. Mechanical strength

Figure 6A shows the mechanical strength as result of the sintering temperature and sintering atmosphere. The lower and upper error bars indicate a cumulative probability of failure of 5% and 95%, respectively. Figure 6B demonstrates in detail how these values were obtained from a Weibull-fit of the cumulative probability of failure to the bending strength (full details in the Supplementary Information).

From the data, it can be concluded that there is no strong influence of the sintering atmosphere on the characteristic strength for the 1000 °C sintered sample. A large reduction in the strength is observed between the fibers sintered up to 1500 °C and at 1790 °C. This loss of strength is attributed to the removal of residual carbon at the higher processing temperatures. As only minor neck formation is present between the silicon carbide particles at these temperatures, the carbon is required to bind together the particles. Although the increasing sintering temperature of 1790 °C increases the inherent strength of the SiC-network through neck formation, this increased strength is offset by the removal of the carbon. A higher sintering temperature of 2075 °C resulted in progressive sintering of the silicon carbide particles, leading to an increasing mechanical strength.

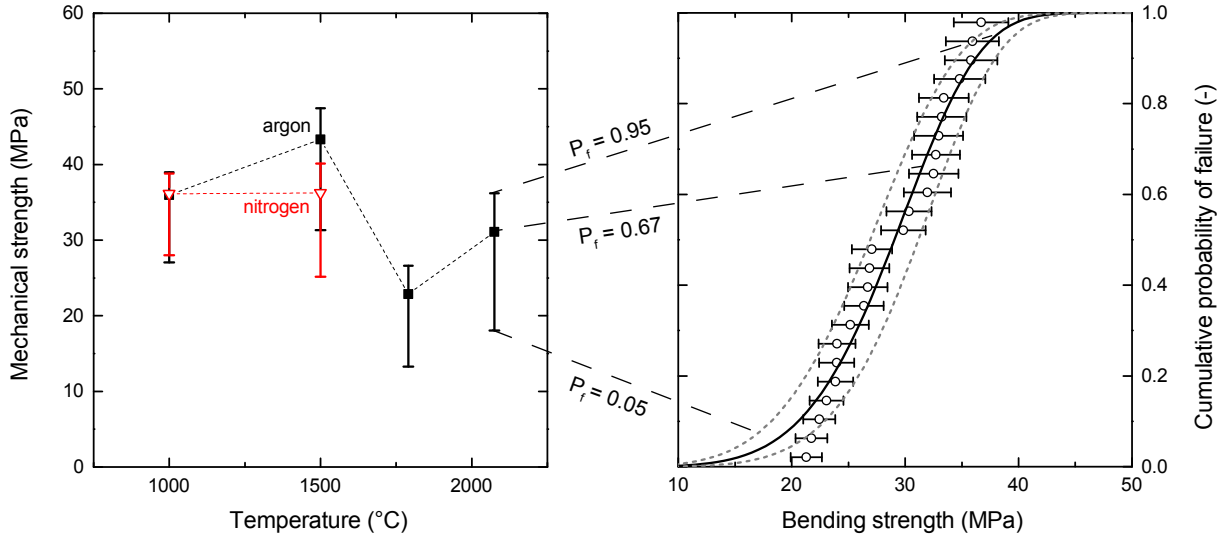

Figure 6: Summary of measured mechanical strengths at different temperature and atmosphere. In A), the symbol (square for argon, triangle for nitrogen) denotes the characteristic strength (σ_θ) from Weibull fitting. The lower error bar denotes the strength at which 5% of the fibers would fail. The upper error bar denotes strength at which 95% of the fibers would fail. B) shows the weibull cumulative probability function for the 2075-Ar sample, showing the measured mechanical strengths where the error bar denotes measurement error. The solid line is the fit based on the weibull function, whereas the dashed lines represent the 95% confidence interval of the fit.

At first glance the mechanical strength of these silicon carbide fibers appears to be low in comparison with other ceramic hollow fibers [18, 37–39]. These values, however, cannot be directly compared as in the present study the bending strength was obtained via a 4-point bending test. This results in a lower value for the mechanical strength as compared to an often-used 3-point bending test [40]. In addition, assessing the mechanical strength of a ceramic based on small sample numbers requires caution as sample-to-sample differences might introduce large errors. Even though in this study a limited sample size of 24 fibers is used [41–43], this method of testing provides a better insight in the mechanical behaviour of these fibers as compared to other studies.

3.3.2. Clean water permeation

Figure 7 shows the clean water permeability for fibers sintered at various temperatures. The fibers sintered at 1000 °C show a clean water permeability of approximately 500 L m^{-2} h^{-1} bar^{-1} for both sintering atmospheres. After sintering at 1500 °C an increase in permeability to values in the order of 1000 L m^{-2} h^{-1} bar^{-1} to 1200 L m^{-2} h^{-1} bar^{-1} is observed. The sintering atmosphere has little influence on the clean water permeability for these fibers.

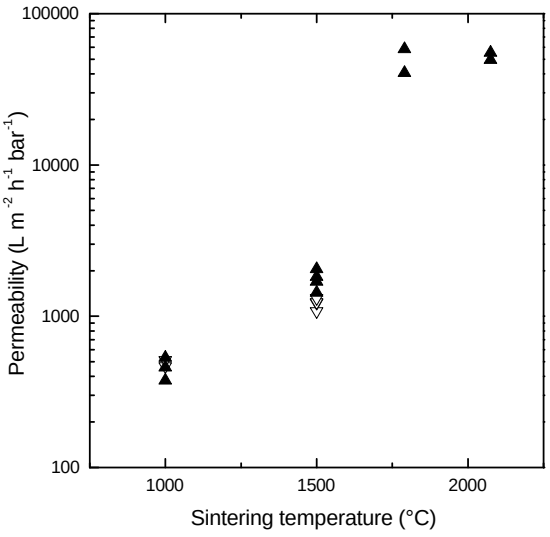

Figure 7: Clean water permeability for silicon carbide fibers sintered at various temperatures. The open symbols represent fibers sintered in a nitrogen atmosphere, the closed symbols represent the fibers sintered in an argon atmosphere. Each symbol represents a single fiber.

After high temperature sintering the clean water permeability increases more than tenfold to values in the order of 50 000 L m^{-2} h^{-1} bar^{-1}. Sintering at these high temperatures not only removed the residual carbon but also resulted in larger pores, yielding this increased clean water permeability. The observed clean water permeability of the fibers in this study (pore size 0.5 µm to 3 µm) is approximately a factor 50 higher than that reported for alumina (pore size 0.1 µm to 1.4 µm) [44, 45], a factor 5 higher than that reported for titanium (pore size 1 µm to 3 µm) [39] and a factor 2 higher than that reported for silicon nitride hollow fibers (pore size 0.5 µm to 0.9 µm) [37].

Burst pressure experiments were conducted up to a transmembrane pressure of 20 bar without rupture of the fiber, further substantiating the mechanical robustness of the fibers. (see the Supplementary Information).

4. Conclusion

Porous silicon carbide hollow fiber membranes with outer diameters of 1.8 mm were prepared successfully by dry-wet spinning followed by a thermal treatment at various temperatures. Tuning of the microstructure by changing the sintering temperature allowed for the optimization of pore size and mechanical strength of the fibers. Although sintering at 1500 °C yielded mechanically stable fibers, the carbon residue of the polymeric binder effectively blocked the pores of the fiber, resulting in low water fluxes. The carbon binds the SiC-particles together, as is evident from the sharp decrease in mechanical strength when carbon is removed upon heating to 1790 °C. A treatment at temperatures as high as 2075 °C is required to sufficiently sinter together the silicon carbide particles. The resulting fibers show exceptionally high clean water fluxes in the order of 50 000 L m^{-2} h^{-1} bar^{-1} at a differential pressure of 1 bar. With pore sizes in the order of microns, the membranes are directly applicable as a microfiltration membrane, or can be used as a substrate for UF or gas-separation membranes.

5. Acknowledgements

This research is supported by the Dutch Technology Foundation STW, which is part of the Netherlands Organisation for Scientific Research (NWO), and which is partly funded by the Ministry of Economic Affairs. This work has been funded within the "Inorganic porous hollow fibers for intensified fractionation and filtration" project by the German Research Foundation (Deutsche Forschungsgemeinschaft - DFG). Matthias Wessling appreciates the financial support from the Alexander-von-Humboldt Foundation.

The authors would like to acknowledge LiqTech International A/S, Denmark for access to their high temperature furnaces.

References

[1] T. Thomé, M. Capelle, L. Thomé, T. Prenant, M. Néret, Thermal Oxidation of Sintered Silicon Carbide Used for Diesel Particulate Filter Walls, Journal of Ceramic Science and Technology 3 (2012) 89–94.

[2] J. A. Díaz, M. Calvo-Serrano, A. R. de la Osa, A. M. García-Minguillán, A. Romero, A. Giroir-Fendler, J. L. Valverde, β-silicon carbide as a catalyst support in the Fischer-Tropsch synthesis: Influence of the modification of the support by a pore agent and acidic treatment, Applied Catalysis A: General 475 (2014) 82–89.

[3] M. Rosso, A. Arafat, K. Schroën, M. Giesbers, C. S. Roper, R. Maboudian, H. Zuilhof, Covalent attachment of organic monolayers to silicon carbide surfaces., Langmuir 24 (2008) 4007–12.

[4] V. Suwanmethanond, E. Goo, P. K. T. Liu, G. Johnston, M. Sahimi, T. T. Tsotsis, Porous silicon carbide sintered substrates for high-temperature membranes, Industrial & Engineering Chemistry Research 39 (2000) 3264–3271.

[5] W. Deng, X. Yu, M. Sahimi, T. T. Tsotsis, Highly permeable porous silicon carbide support tubes for the preparation of nanoporous inorganic membranes, Journal of Membrane Science 451 (2014) 192–204.

[6] S. Chae, Y. Kim, I. Song, Porosity control of porous silicon carbide ceramics, Journal of the European Ceramic Society 29 (2009) 2867–2872.

[7] F. Chen, R. Mourhatch, T. T. Tsotsis, M. Sahimi, Experimental studies and computer simulation of the preparation of nanoporous silicon-carbide membranes by chemical-vapor infiltration/chemical-vapor deposition techniques, Chemical Engineering Science 63 (2008) 1460–1470.

[8] B. Elyassi, W. Deng, M. Sahimi, T. T. Tsotsis, On the use of porous and nonporous fillers in the fabrication of silicon carbide membranes, Industrial & Engineering Chemistry Research 52 (2013) 10269–10275.

[9] B. Hofs, J. Ogier, D. Vries, E. F. Beerendonk, E. R. Cornelissen, Comparison of ceramic and polymeric membrane permeability and fouling using surface water, Separation and Purification Technology 79 (2011) 365–374.

[10] Liqtech, Success for LiqTech ceramic membranes in oil & gas trial, Filtration Industry Analyst 2012 (2012) 4.

[11] Veolia Water Solutions and Technology, Veolia adds silicon carbide membranes to its CeraMem range, Membrane Technology 2010 (2010) 4.

[12] R. Neufert, M. Moeller, A. Bakshi, Dead-end silicon carbide micro-filters for liquid filtration, in: R. Narayan, P. Colombo, S. Kirihar, S. Widjaja (Eds.), Advances in Bioceramics and Porous Ceramics VI, John Wiley & Sons, Inc., Hoboken, NJ, USA, 2013.

[13] P. Lin, D. Tsai, Preparation and analysis of a silicon carbide composite membrane, Journal of the American Ceramic Society 72 (1997) 365–372.

[14] M. Facciotti, V. Boffa, G. Magnacca, L. B. Jø rgensen, P. K. Kristensen, A. Farsi, K. König, M. L. Christensen, Y. Yue, Deposition of thin ultrafiltration membranes on commercial SiC

microfiltration tubes, Ceramics International 40 (2014) 3277–3285.
[15] X. Tan, S. Liu, K. Li, Preparation and characterization of inorganic hollow fiber membranes, Journal of Membrane Science 188 (2001) 87–95.
[16] J. de Jong, N. Benes, G. Koops, M. Wessling, Towards single step production of multi-layer inorganic hollow fibers, Journal of Membrane Science 239 (2004) 265–269.
[17] S. Husain, W. J. Koros, Macrovoids in Hybrid Organic/Inorganic Hollow Fiber Membranes, Industrial & Engineering Chemistry Research 48 (2009) 2372–2379.
[18] S. Liu, K. Li, R. Hughes, Preparation of porous aluminium oxide (Al2O3) hollow fibre membranes by a combined phase-inversion and sintering method, Ceramics International 29 (2003) 875–881.
[19] R. Terpstra, J. V. Eijk, F. Feenstra, Method for the production of ceramic hollow fibres, US Patent 5,707,584 (1998).
[20] D.-G. Shin, E.-B. Kong, K.-Y. Cho, W.-T. Kwon, Y. Kim, S.-R. Kim, J.-S. Hong, D.-H. Riu, Nano-Structure Control of SiC Hollow Fiber Prepared from Polycarbosilane, Journal of the Korean Ceramic Society 50 (2013) 301–307.
[21] M. W. J. Luiten-olieman, M. J. T. Raaijmakers, L. Winnubst, T. C. Bor, M. Wessling, A. Nijmeijer, N. E. Benes, Towards a generic method for inorganic porous hollow fibers preparation with shrinkage-controlled small radial dimensions , applied to Al 2 O 3 , Ni , SiC , stainless steel , and YSZ, Journal of Membrane Science 407-408 (2012) 155–163.
[22] M. Luiten-Olieman, L. Winnubst, A. Nijmeijer, M. Wessling, N. E. Benes, Porous stainless steel hollow fiber membranes via drywet spinning, Journal of Membrane Science 370 (2011) 124–130.
[23] The MathWorks, MATLAB and Optimization Toolbox, Release 2012b, 2012.
[24] C. León, New perspectives in mercury porosimetry, Advances in colloid and interface science 66-77 (1998) 341–372.
[25] ASTM, C1161-02 Standard Test Method for Flexural Strength of Advanced Ceramics at Ambient Temperature, ASTM International, West Conshohocken, PA (2002) 1–21.
[26] B. Kingsbury, K. Li, A morphological study of ceramic hollow fibre membranes, Journal of Membrane Science 328 (2009) 134–140.
[27] Y. Gupta, A. Chakraborty, Thermal and thermooxidative degradation of engineering thermoplastics and life estimation, Journal of Applied Polymer Science 92 (2004) 1737–1748.
[28] X.-G. Li, H.-T. Shao, H. Bai, M.-R. Huang, W. Zhang, High-resolution thermogravimetry of polyethersulfone chips in four atmospheres, Journal of Applied Polymer Science 90 (2003) 3631–3637.
[29] L.-H. Perng, Comparison of thermal degradation characteristics of poly(arylene sulfone)s using thermogravimetric analysis/mass spectrometry, Journal of Applied Polymer Science 81 (2001) 2387–2398.
[30] J. Baird, J. Taylor, Reaction between silica and carbon and the activity of silia in slag solution, Transactions of the Faraday Society 54 (1958) 526–539.
[31] A. Kaza, M. J. Matthewson, D. Niesz, R. L. Haber, M. A. Rossi, A Model of Gas-Phase Transport During the Initial Stages of Sintering of Silicon Carbide, Journal of the American Ceramic Society 92 (2009) 2517–2527.
[32] W. Rijswijk, D. Shanefield, Effects of carbon as a sintering aid in silicon carbide, Journal of the American Ceramic Society (1990).
[33] A. Malinge, A. Coupé, Y. Le Petitcorps, R. Pailler, Pressureless sintering of beta silicon carbide nanoparticles, Journal of the European Ceramic Society 32 (2012) 4393–4400.
[34] W. Hertl, W. Pultz, Disproportionation and Vaporization of Solid Silicon Monoxide, Journal of the American Ceramic Society 50 (1967) 278–381.
[35] M. Morgan, Conduction in amorphous carbon films, Thin Solid Films 7 (1970) 313–323.
[36] S. Prochazka, Sintered dense silicon carbide, US Patent 4,004,934 (1977).
[37] J.-W. Zhang, H. Fang, J.-W. Wang, L.-Y. Hao, X. Xu, C.-S. Chen, Preparation and characterization of silicon nitride hollow fiber membranes for seawater desalination, Journal of Membrane Science 450 (2014) 197–206.
[38] X. Zhang, D. K. Wang, D. R. S. Lopez, J. a. C. Diniz da Costa, Fabrication of nanostructured TiO2 hollow fiber photocatalytic membrane and application for wastewater treatment, Chemical Engineering Journal 236 (2014) 314–322.
[39] O. David, Y. Gendel, M. Wessling, Tubular macro-porous titanium membranes, Journal of Membrane Science 461 (2014) 139–145.
[40] J. B. Wachtman, W. Roger Cannon, M. John Matthewson, Mechanical properties of ceramics, John Wiley & Sons, Inc., 1996.
[41] C. Lu, R. Danzer, F. Fischer, Fracture statistics of brittle materials: Weibull or normal distribution, Physical Review E 65 (2002) 067102.
[42] T. Hoshide, H. Sugiyama, Numerical Analysis of Sample-Size Effect on Strength of Alumina, Journal of Materials Engineering and Performance 22 (2012) 1–8.
[43] I. Štubna, P. Šín, A. Trník, L. Vozár, Measuring the Flexural Strength of Ceramics at Elevated TemperaturesAn Uncertainty Analysis, Measurement Science Review 14 (2014) 35–40.
[44] M. Lee, Z. Wu, R. Wang, K. Li, Micro-structured alumina hollow fibre membranes Potential applications in wastewater treatment, Journal of Membrane Science 461 (2014) 39–48.
[45] G. Xu, K. Wang, Z. Zhong, C.-s. Chen, P. a. Webley, H. Wang, SiC nanofiber reinforced porous ceramic hollow fiber membranes, Journal of Materials Chemistry A 2 (2014) 5841.